Degenerate Four-Wave Mixing in a Multiresonant Germanium Nanodisk

Gustavo Grinblat, Yi Li*, Michael P. Nielsen, Rupert F. Oulton, Stefan A. Maier*

The Blackett Laboratory, Department of Physics, Imperial College London, London SW7 2AZ, United Kingdom

ABSTRACT. Dielectric nanoantennas excited at Mie resonances are becoming suitable candidates for nonlinear optical effects due to their large intrinsic nonlinearity and capability to highly confine electromagnetic fields within subwavelength volumes. In this work, we show that a single Ge nanodisk, recently demonstrated as an efficient source of third harmonic generation (THG), can also be exploited for four-wave mixing (FWM) phenomena. The high field enhancement inside the disk yields effective third-order susceptibilities as high as 2×10^{-8} esu (2.8×10^{-16} m^2/V^2), which were determined by single pump wavelength THG measurements tuned to high-order Mie modes. A similar nonlinear optical response is observed in the case of degenerate FWM where two different pump wavelengths are coupled to a single high-order resonant mode. However, when the two pump wavelengths are coupled to different high order modes, the FWM process is partially suppressed due to a diminished near-field spatial overlap of the mixed wavelengths within the disk. This investigation reveals useful pathways for the optimization of third-order optical processes in all-dielectric nanostructures.

KEYWORDS: dielectric nanoantennas; Mie resonances; field enhancement; third harmonic generation; four-wave mixing.

High-resolution optical microscopy,[1-4] ultra-sensitive nanoscale sensing,[5,6] photonic nanocircuitry,[7] and optoelectronic nanodevices,[8] can all be boosted by exploiting nonlinear optical effects with large efficiencies at subwavelength volumes. In most cases, nonlinear optical phenomena involve the interaction of two or more photons in a nonlinear medium to produce one or more photons at different energies. As a consequence, the intensity of the generated light often depends in a superlinear manner on the input field intensity, allowing this kind of processes to be enhanced by locally confining electromagnetic fields to maximize the excitation density. An example of such a nonlinear optical effect is third harmonic generation (THG), which coherently combines three photons of equal frequency to create a new photon of triple the incident photon frequency.[9-11] In this situation, the generated light intensity increases with the cube of the input excitation power, and relies on the third order susceptibility of the material, $\chi^{(3)}$.

A larger number of photon frequencies can be processed by four-wave mixing (FWM),[12-14] a third-order nonlinear effect in which two or three different incident photon energies are mixed, enabling multiple output wavelengths. In particular, when three different incident photon frequencies are considered ($\omega_1 \neq \omega_2 \neq \omega_3$), a non-degenerate process takes place, producing five different waves governed by the equation $\omega_{FWM} = \pm \omega_1 \pm \omega_2 \pm \omega_3$. In the case of only two incident frequencies ω_1 and ω_2, degenerate FWM gives rise to four different generated frequencies $\omega_{FWM} = 2\omega_{1,2} \pm \omega_{2,1}$. To differentiate between the "+" and "-" cases, some authors refer to them as "four-wave sum mixing" and "four-wave difference mixing", respectively.[15,16]

When all incident photons have identical frequency ω, the process simplifies to $\omega_{FWM} = 3\omega$, i.e. the THG phenomenon.

Numerous examples of FWM processes on the nanoscale have been demonstrated via plasmonic nanoantennas during the past decade.[17-21] Radiative electric modes have been engineered to concentrate the fundamental fields in the vicinity of metallic nanoclusters to maximize their nonlinear optical response. However, intrinsic ohmic losses, together with a field confinement effect that is limited to surfaces, severely restrict the conversion efficiencies that can be attained with plasmonic nanoantennas.[22-25] To address this issue, more recently, low-loss dielectric nanoantennas made of Si or Ge have been investigated for enhanced nonlinear processes due to their large intrinsic nonlinear index, multiple resonant modes, and ability to concentrate fields within their volumes.[26-30] Remarkably, THG conversion efficiencies of the order of 10^{-3}% have been demonstrated for single Ge nanodisks when exciting at higher-order anapole modes[30]. However, up until now, FWM processes have not been effectively manipulated in single dielectric nanostructures.

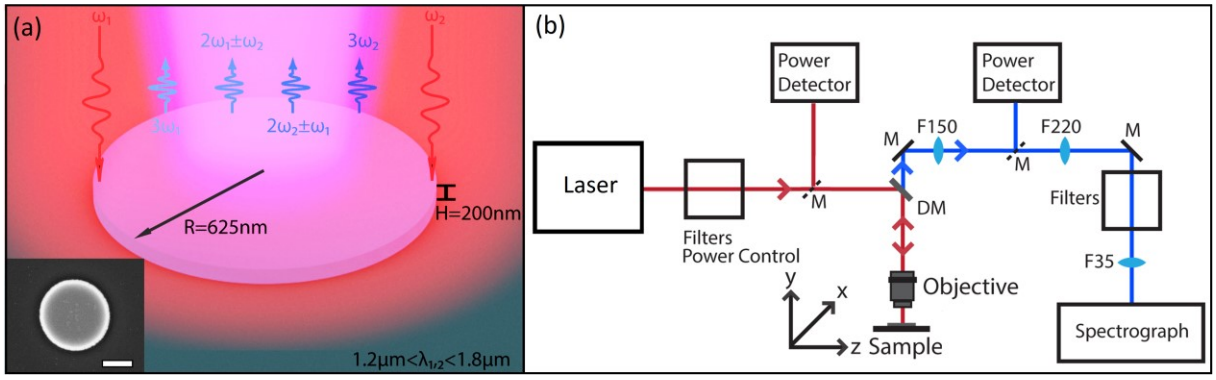

Figure 1. *(a) Illustration of the nonlinear experiment. A 200 nm-thick Ge disk on glass is excited with one or more photon energies using ultrafast near-infrared light. The inset shows a representative scanning electron microscope (SEM) image of the nanodisk. Scale bar, 500 nm.*

(b) Schematic of the experimental setup. 'M' denotes a mirror, 'DM' denotes a dichroic mirror, and 'FXXX' denotes a lens with focal length XXX in mm. For the mirrors, dashed lines represent flipper mirrors. The light source was focused on the sample through a high numerical aperture objective and the sample was then scanned using a three-axis stage. A shortpass dichroic mirror removes the pump beam from the nonlinear output, which is then measured with either a power detector or a spectrograph.

In this work, we analyze the degenerate FWM performance of a single Ge nanodisk in the visible range when exciting with fundamental wavelengths in the near-infrared region (i.e., the four-wave sum mixing case), as schematized in Figure 1. First, the presence of resonances that enhance the electric energy inside the structure is identified through extinction and THG measurements. Then, the FWM process is characterized using two excitation beams, and the comparison is made between the FWM signals when exciting at a single high-order resonant mode and when combining two high-order resonant modes. The results show that the best efficiency is achieved when the near-field overlap of the incident wavelengths inside the nanostructure is maximized.

Ge disks of 200 nm height and 625 nm radius were fabricated by means of electron beam lithography and a standard lift-off process (see Methods section for fabrication details). A pitch of 4 μm was chosen to avoid optical coupling between adjacent disks. The extinction cross section of the particles was studied by Fourier transform infrared (FTIR) spectroscopy in arrays of 25 × 25 disks in transmission configuration. At the same time, to theoretically analyze the experimental results, simulations were performed using the RF module of Comsol software (refer to Methods for details on simulations and optical characterization). Figure 2 a-b show, respectively, the result of extinction measurements together with the corresponding numerical

calculation. A good agreement is observed between the curves, however there are some discrepancies which may be attributed to small variations among different disks due to imperfections in the fabrication process.[26,27,32] In addition, the use of a reflective microscope objective in the collection geometry could also have contributed to this disagreement, as this type of objective blocks the central region of the beam and may alter the relative contribution of the different modes to the spectrum. We note that the characteristic anapole mode of the disk is located beyond 2000 nm wavelength (region not shown), and therefore the spectra in Figure 2 comprise only higher-order modes, which have been recently demonstrated as the most efficient for THG in a dielectric disk.[30] The near-field intensity distribution at mid-height of the disk is represented in Figure 2 d-e for three different wavelengths in the spectrum, labelled as HOM1, HOM2, and HOM3. In all cases, we observe that the electric field is preferentially located inside the antenna, which is a beneficial aspect for nonlinear processes with large volume contribution such as THG and FWM.

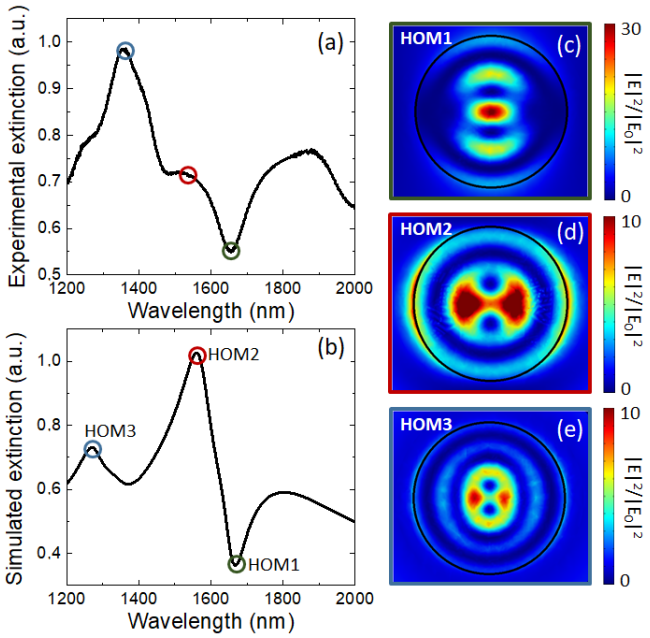

Figure 2. ***(a)*** *Experimental and* ***(b)*** *simulated extinction spectra of a Ge disk of 200 nm height and 625 nm radius. The experimental cross sections correspond to measured values of 1-T (T, transmittance).* ***(c)-(e)*** *Simulated distribution of the electric field intensity ($|E|^2/|E_0|^2$) computed inside the nanodisk and its surroundings for the modes HOM1 (c), HOM2 (d), and HOM3 (e).*

To confirm that the observed resonant modes indeed maximize the electric energy within the Ge particle, we studied the THG response when exciting at varying fundamental wavelength λ_{pump} (refer to Methods for experimental details on the nonlinear characterization). Figure 3a shows the measured THG spectra (red curves) for λ_{pump} in the 1250-1750 nm range. It is found that the envelope of the spectra (black curve) presents three distinctive peaks, indicating high field enhancement inside the disk. To theoretically describe this result, considering that THG is a third-order process, we analyzed the spectral dependence of the cube of the electric energy stored within the particle at the fundamental wavelength. The electric energy was computed as $W_E = n^2 \iiint |E|^2 \, dV/2$, where n and V denote the refractive index and volume of the dielectric particle, respectively. We remark that no resonances were found at the THG wavelengths and therefore no significant contribution to the enhancement effect is expected to originate from the emission process. As shown in Figure 3b, a very good agreement is obtained between simulation and experiment, with the three maxima in $(W_E)^3$ occurring at the λ_{pump} wavelengths corresponding to the modes HOM1, HOM2, and HOM3 as anticipated. Regarding the difference in intensity between experiment and simulation for the peak at the shortest (fundamental) wavelength, it may be attributed to the decreasing $\chi^{(3)}$ behavior with decreasing wavelength for Ge in this spectral region,[33] which reduces the nonlinear performance. In order to quantify the nonlinear response of the Ge nanodisk in the optimal condition, we studied the power dependence of the nonlinear signal at λ_{pump} = 1650 nm. As shown in the inset of Figure 3(a), the expected cubic trend is

observed, giving rise to a maximum THG conversion efficiency of η_{THG} ~10^{-3}% (η_{THG} = THG power/excitation power) at a peak pump intensity of 8 GW/cm^2. To compute an effective value of the third-order nonlinear susceptibility for the nanodisk, we consider first that the THG signal power, P_{THG}, is proportional to the cube of the pump power, P_{pump}, with $(\chi^{(3)})^2$ as the proportionality coefficient, i.e. $P_{THG} \propto (\chi^{(3)})^2 * (P_{pump})^3$. Then, by comparing the THG response of the disk with that of bulk Ge,[27] the effective nonlinear susceptibility $\chi_{eff}^{(3)}$ of the particle is determined to be as large as 2×10^{-8} esu (2.8×10^{-16} m^2/V^2), which is 2 orders of magnitude larger than that of the bulk. Moreover, we estimate that this value could be as high as ~10^{-15} m^2/V^2 if the disk radius is increased to about 1 μm so that the HOM1 resonance occurs at around 2500 nm wavelength, i.e. where the intrinsic nonlinear response from Ge is maximum.[33] This would further enhance η_{THG} by nearly two orders of magnitude. It is worth mentioning here that the obtained $\chi_{eff}^{(3)}$ is up to one order of magnitude lower than those reported for plasmonic nanoantennas.[18] Indeed, third-order susceptibilities of metals are among the highest in nature.[34] Nevertheless, since plasmonic nanostructures confine electromagnetic fields exclusively to surfaces, their corresponding third-order optical efficiencies (i.e., η_{THG}) are reported to be several orders of magnitude smaller than the one presented here,[35-39] leaving the dielectric strategy as the best approach.

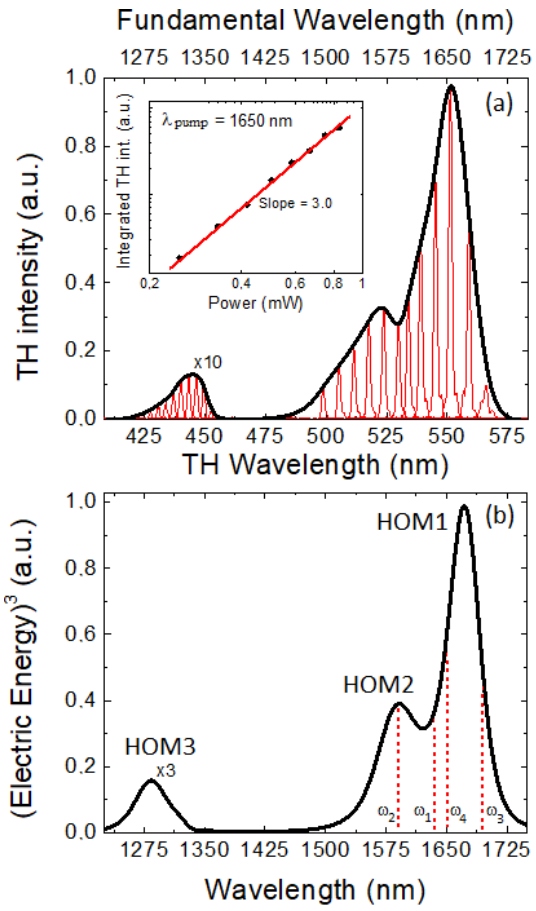

Figure 3. ***(a)*** *Fundamental wavelength dependence of the THG spectrum for the Ge disk. Each spectrum (red curves) corresponds to a different fundamental wavelength of triple that of the central THG wavelength. The envelope of the set of spectra is shown in black. The inset exhibits the measured excitation power dependence of the THG signal at 1650 nm pump wavelength. The line in the plot is a fit considering cubic dependence with the excitation power.* ***(b)*** *Simulated spectral dependence of the cube of the electric energy (W_E) inside the disk. The dashed lines represent the excitation frequencies chosen for the FWM studies.*

Due to the presence of several resonances in the Ge disk, we could study FWM by exciting either multiple or single modes. In particular, from the results in Figure 3, HOM1 and HOM2 are expected to be the best candidates to be used for FWM processes since their THG signals are

found to be the highest. In addition, these two modes were estimated to have a field intensity overlap as high as ~80% within the disk, enabling efficient wave mixing effects.[18] The combination of highly confined fields and spatial overlap of HOM1 and HOM2 within the disk with low absorption[40] should allow FWM processes to be effectively exploited.

Figure 4a shows the result of mixing two different excitation frequencies, one at HOM1 and one at HOM2, namely ω_1 and ω_2 respectively. Excitation powers for the different wavelengths were adjusted to produce similar THG responses (corresponding peaks are labelled as $3\omega_1$ and $3\omega_2$ in the graph). As it can be seen in the figure, two additional maxima appear in between the two THG peaks. When calculating the associated frequencies, it is found that those maxima correspond to the FWM signals at $2\omega_1 + \omega_2$ and $2\omega_2 + \omega_1$ (i.e., the four-wave sum mixing process). Interestingly, it is observed that the intensities of the FWM peaks are >30% lower than those related to the THG emission, indicating that it is not equivalent to mix photons of different or equal frequencies. To analyze this result theoretically, we have estimated the nonlinear cross-sections of the near fields inside the disk for the FWM process. To that end, we have calculated the volume integral of the products $P_{12,21} = \left|E_{\omega 1,2}\right|^4 \times \left|E_{\omega 2,1}\right|^2$ inside the disk, after corroborating the expected quadratic and linear dependencies of the FWM signals with the intensities of the fundamental fields (inset of Figure 4(a)). Figure 4 b-c exhibit 2D distributions of the nonlinear cross-sections at mid-height of the disk prior to volume integration. Combinations of the patterns corresponding to the different modes involved (Figure 2 b-c) can be appreciated. After volume integration of $P_{12,21}$, the obtained values are found to be ~40% lower than those for the THG processes. This proportional reduction in response due to the reduced spatial mode overlap is in good agreement with the experimental results considering the mixing of the various combinations of three photons at ω_1 and ω_2. To further confirm this observation,

the two different pump frequencies, namely ω_3 and ω_4, were coupled to a single high order mode. The reduction in the FWM signals with respect to the THG peaks is now significantly less than in the multi-mode FWM case, as shown in Figure 4d for HOM1. This can be understood from the much better overlap between the near field distributions at the two selected frequencies, which approaches 100% since the patterns are in this case essentially the same. We remark that the mode engineering approach proposed here would also be useful for the FWM emissions at $2\omega_{1,2} - \omega_{2,1}$ and $2\omega_{3,4} - \omega_{4,3}$, since their efficiencies depend on the near-field overlap of the excitation waves in the same way as the analyzed "+" cases.[18]

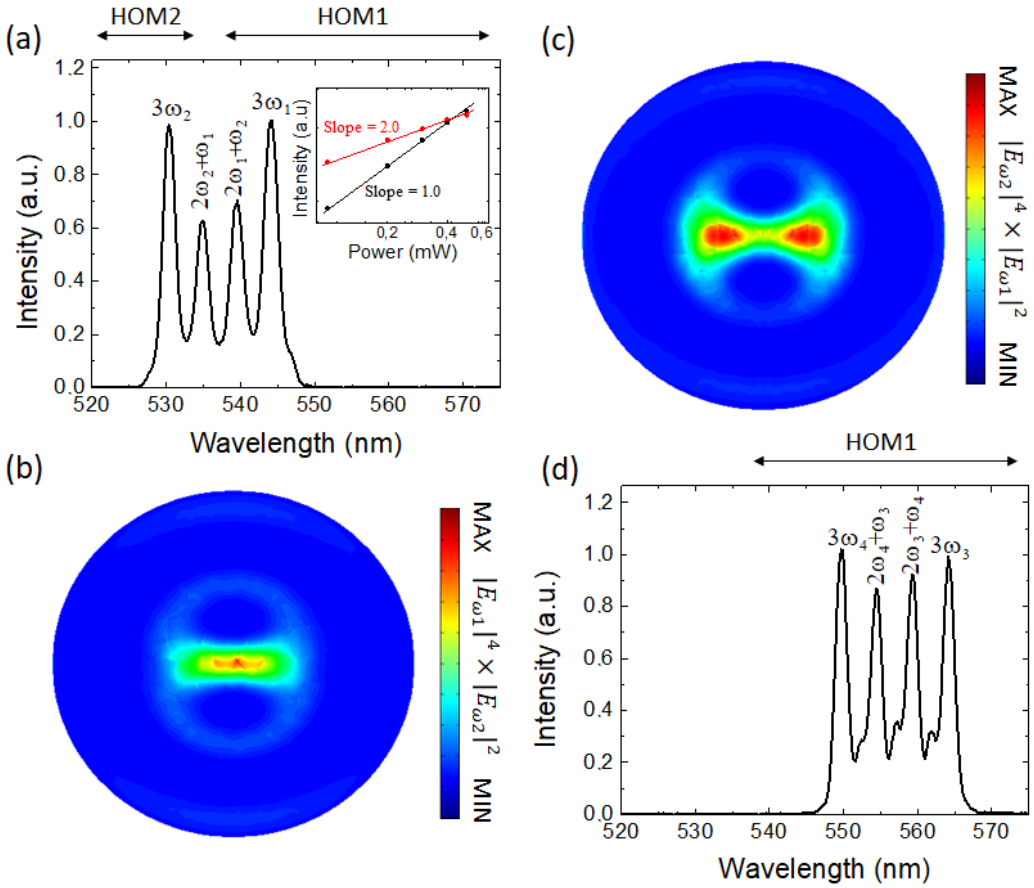

Figure 4. ***(a)*** *Measured nonlinear response of the Ge disk when exciting at HOM1 and HOM2 modes simultaneously. The inset exhibits the dependence of the FWM signal at* $2\omega_1 + \omega_2$ *with the*

excitation powers. A quadratic (linear) behavior with the pump power at ω_1 (ω_2) is observed. ***(b)-(c)*** *Nonlinear cross-section maps for the FWM process when mixing the modes HOM1 and HOM2.* ***(d)*** *Measured nonlinear response of the Ge disk when exciting at two different wavelengths comprised by HOM1.*

In conclusion, FWM processes with emission at visible frequencies were studied by exciting a single Ge nanodisk at multiple high-order modes in the near-infrared range. When considering a single excitation frequency, the third order susceptibility was found to be as large as 2×10^{-8} esu (2.8×10^{-16} m^2/V^2), which is two orders of magnitude greater than the corresponding value for bulk Ge. When mixing two pump wavelengths comprised by a single high-order mode, the degenerate FWM signals were observed to decrease by only ~10% in intensity with respect to the THG process, indicating nearly equivalent efficiency. However, when considering two different modes with near-field intensity overlap of about 80% within the disk, the FWM peaks were found to be >30% lower in intensity compared to the THG case. These results show that the single dielectric nanodisk operating at high-order modes works as an efficient element for FWM processes in subwavelength volumes.

METHODS

Sample Fabrication. Arrays of Ge nanodisks with 4 μm pitch and radius of 625 nm were fabricated on borosilicate glass using electron beam lithography. The substrate was first coated with positive-tone PMMA (950K A4) resist, and posteriorly baked for 5 minutes at 180 °C. The nanostructures were then defined by an electron beam exposure, followed by a development procedure. Ge thermal evaporation at 1.5 Å/s at room temperature (resulting in amorphous Ge growth) and a standard lift-off process completed the fabrication process.

Optical Characterization. Extinction measurements of the fabricated nanoantennas were performed *via* FTIR spectroscopy (Bruker Hyperion 2000) using linearly polarized light at normal incidence in transmission mode, averaging over arrays of 25×25 disks. 36 X (NA = 0.5) reflective objectives were used to focus and collect the light. For the THG characterization of individual nanostructures, a pulsed Yb:KGW PHAROS laser system was used as the pump of a collinear optical parametric amplifier ORPHEUS with a LYRA wavelength extension option (Light Conversion Ltd, pulse duration of 180 fs, repetition rate of 100 kHz). The excitation beam (λ = 1200 nm - 1800 nm) was reflected by a shortpass dichroic mirror (Thorlabs DMSP1000) and focused onto a 1.2 μm^2 spot on the sample with a 100X (NA = 0.9) air objective from Nikon. The THG emission was collected in a back-scattering configuration *via* the same objective, and detected with a spectrograph (PI Acton SP2300 by Princeton Instruments) for spectral measurements. The sample was fixed to an XYZ piezo-scanner stage (Nano-Drive, Mad City Labs) to perform the scanning. The power of the collected THG emission was measured with a calibrated silicon photodetector (Newport), and the excitation power was measured with a germanium photodetector (Thorlabs). For <1 pW THG powers, values were calibrated by using the measured THG spectra. For the FWM studies, a supercontinuum laser (SC400, NKT Photonics) coupled to an acousto-optic tunable filter (SuperK SELECT, NKT Photonics) that allowed multiple excitation wavelengths simultaneously was employed.

Numerical Simulations. Theoretical calculations of the extinction cross section spectra and the near-field intensity distributions were performed using the RF module of the commercial software *Comsol Multiphysics*. Simulations were carried out within a 4 μm diameter sphere containing the Ge nanodisk on glass substrate and surrounded by air medium. The problem was solved for the scattered field using scattering boundary conditions and a perfectly matched layer

of 50 nm thickness. The extinction cross section was calculated as the sum of the absorption and scattering cross sections, *i.e.* $\sigma_{ext} = \sigma_{abs} + \sigma_{scat}$, considering linearly polarized light at normal incidence. The absorption cross section was computed over the nanodisk volume, while the scattering cross section was calculated as the field scattered over a semi-sphere placed opposite to the direction of incidence of the pump wave. In order to account for small deviations of the fabricated structure from the perfect cylinder, we have allowed variations in the radius of around 10% in the numerical calculations to better describe the experimental results. Simulations of the electric energy stored inside the nanostructure were performed by integrating the electric field intensity within the nanodisk volume using the expression $W_E = n^2 \iiint |E|^2 \, dV/2$. Similarly, the nonlinear cross-sections for the FWM processes were calculated by integrating the products $\left|E_{\omega 1,2}\right|^4 \times \left|E_{\omega 2,1}\right|^2$ considering the selected wavelengths at the modes HOM1 and HOM2, correspondingly.

AUTHOR INFORMATION

Corresponding Authors

g.grinblat@imperial.ac.uk, yi.li@imperial.ac.uk

Author Contributions

G. G. and Y. L. contributed equally to this work.

Notes

The authors declare no competing financial interest.

ACKNOWLEDGMENTS

The authors acknowledge funding provided by the EPSRC Reactive Plasmonics Programme (EP/M013812/1), the EPSRC Mathematical Fundamentals of Metamaterials Programme (EP/L024926/1), ONR Global, the Royal Society, and the Lee-Lucas Chair in Physics. G. G. further acknowledges a Marie Skłodowska-Curie Fellowship. Requests for data should be sent to datainquiryEXSS@imperial.ac.uk.

REFERENCES

(1) Min, W.; Lu, S.; Rueckel, M.; Holtom, G. R.; Xie, X. S. Near-Degenerate Four-Wave-Mixing Microscopy. *Nano Lett.* **2009**, *9*, 2423-2426.

(2) Kravtsov, V.; Ulbricht, R.; Atkin, J. M.; Raschke, M. B. Plasmonic Nanofocused Four-Wave Mixing For Femtosecond Near-Field Imaging. *Nature Nanotech.* **2016**, *11*, 459-464.

(3) Latour, G.; Robinet, L.; Dazzi, A.; Portier, F.; Deniset-Besseau, A.; Schanne-Klein, M. C. Correlative Nonlinear Optical Microscopy and Infrared Nanoscopy Reveals Collagen Degradation in Altered Parchments. *Sci. Rep.* **2016**, *6*, 26344.

(4) Streets, A. M.; Li, A.; Chen, T.; Huang, Y. Imaging without Fluorescence: Nonlinear Optical Microscopy for Quantitative Cellular Imaging. *Anal. Chem.* **2014**, *86*, 8506–8513.

(5) Butet, J.; Russier-Antoine, I.; Jonin, C.; Lascoux, N.; Benichou, E.; Brevet, P. F. Sensing with Multipolar Second Harmonic Generation from Spherical Metallic Nanoparticles. *Nano Lett.* **2012**, *12*, 1697-1701.

(6) Butet, J.; Lovera, A.; Martin, O. J. Detecting the Trapping of Small Metal Nanoparticles in the Gap of Nanoantennas with Optical Second Harmonic Generation. *Opt. Exp.* **2013**, *21*, 28710-28718.

(7) Sun, Y.; Edwards, B.; Alù, A.; Engheta, N. Experimental Realization of Optical Lumped Nanocircuits at Infrared Wavelengths. *Nature Mat.* **2012**, *11*, 208-212.

(8) Seyler, K. L., Schaibley, J. R., Gong, P., Rivera, P., Jones, A. M., Wu, S.; Yan, J.; Mandrus, D. G.; Yao, W.; Xu, X. Electrical Control of Second-Harmonic Generation in a WSe_2 Monolayer Transistor. *Nature Nanotech.* **2015**, *10*, 407-411.

(9) Efimov, A.; Taylor, A. J.; Omenetto, F. G.; Knight, J. C.; Wadsworth, W. J.; Russell, P. S. J. Phase-Matched Third Harmonic Generation in Microstructured Fibers. *Opt. Express* **2003**, *11*, 2567− 2576.

(10) Sasagawa, K.; Tsuchiya, M. Highly Efficient Third Harmonic Generation in a Periodically Poled MgO:$LiNbO_3$ Disk Resonator. *Appl. Phys. Express* **2009**, *2*, 122401.

(11) Miyata, K.; Petrov, V.; Noack, F. High-Efficiency Single-Crystal Third-Harmonic Generation in BiB_3O_6. *Opt. Lett.* **2011**, *36*, 3627− 3629.

(12) Fukuda, H.; Yamada, K.; Shoji, T.; Takahashi, M.; Tsuchizawa, T.; Watanabe, T.; Takahashi, J.; Itabashi, S. I. Four-Wave Mixing in Silicon Wire Waveguides. *Opt. Express* **2005**, *13*, 4629-4637.

(13) Sharping, J. E.; Fiorentino, M.; Coker, A.; Kumar, P.; Windeler, R. S. Four-Wave Mixing in Microstructure Fiber. *Opt. Lett.* **2001**, *26*, 1048-1050.

(14) Xu, X.; Yao, Y.; Zhao, X.; Chen, D. Multiple Four-Wave-Mixing Processes and their Application to Multiwavelength Erbium-Doped Fiber Lasers. *J. Lightwave Technol.* **2009**, *27*, 2876-2885.

(15) Al-Basheer, W.; Hedén, M.; Cai, Z. J.; Shi, Y. J. Study of Two-Photon Resonant Four-Wave Sum Mixing in Xenon in the Spectral Region of 105–110 nm. *Chem. Phys.* **2011**, *381*, 59–66.

(16) Tomkins, F. S.; Mahon, R. High-Efficiency Four-Wave Sum and Difference Mixing in Hg Vapor. Opt. Lett. **1981**, 6, 179-181.

(17) Danckwerts, M.; Novotny, L. Optical Frequency Mixing at Coupled Gold Nanoparticles. *Phys. Rev. Lett.* **2007**, *98*, 026104.

(18) Zhang, Y.; Wen, F.; Zhen, Y. R.; Nordlander, P.; Halas, N. J. Coherent Fano Resonances in a Plasmonic Nanocluster Enhance Optical Four-Wave Mixing. *Proc. Natl. Acad. Sci.* **2013**, *110*, 9215-9219.

(19) Maksymov, I. S.; Miroshnichenko, A. E.; Kivshar, Y. S. Cascaded Four-Wave Mixing in Tapered Plasmonic Nanoantenna. *Opt. Lett.* **2013**, *38*, 79-81.

(20) Hagman, H.; Bäcke, O.; Kiskis, J.; Svedberg, F.; Jonsson, M. P.; Höök, F.; Enejder, A. Plasmon-Enhanced Four-Wave Mixing by Nanoholes in Thin Gold Films. *Opt. Lett.* **2014**, *39*, 1001-1004.

(21) Hasan, S. B.; Lederer, F.; Rockstuhl, C. Nonlinear Plasmonic Antennas. *Mater. Today* **2014**, *17*, 478-485.

(22) Caldarola, M.; Albella, P.; Cortes, E.; Rahmani, M.; Roschuk, T.; Grinblat, G.; Oulton, R. F.; Bragas, A. V.; Maier, S. A. Non-Plasmonic Nanoantennas for Surface Enhanced Spectroscopies with Ultra-Low Heat Conversion. *Nat. Commun.* **2015**, *6*, 7915.

(23) Aouani, H.; Rahmani, M.; Navarro-Cía, M.; Maier, S. A. Third Harmonic-Upconversion Enhancement from a Single Semiconductor Nanoparticle Coupled to a Plasmonic Antenna. *Nat. Nanotechnol.* **2014**, *9*, 290−294.

(24) Halas, N. J.; Lal, S.; Chang, W.-S.; Link, S.; Nordlander, P. Plasmons in Strongly Coupled Metallic Nanostructures. *Chem. Rev.* **2011**, *111*, 3913−3961.

(25) Giannini, V.; Fernandez-Domínguez, A. I.; Heck, S. C.; Maier, S. A. Plasmonic Nanoantennas: Fundamentals and their Use in Controlling the Radiative Properties of Nanoemitters. *Chem. Rev.* **2011**, *111*, 3888−3912.

(26) Shcherbakov, M. R.; Neshev, D. N.; Hopkins, B.; Shorokhov, A. S.; Staude, I.; Melik-Gaykazyan, E. V.; Decker, M.; Ezhov, A. A.; Miroshnichenko, A. E.; Brener, I.; Fedyanin, A. A.; Kivshar, Y. S. Kivshar. Enhanced Third-Harmonic Generation in Silicon Nanoparticles Driven by Magnetic Response. *Nano Lett.* **2014**, *14*, 6488− 6492.

(27) Grinblat, G.; Li, Y.; Nielsen, M.; Oulton, R. F.; Maier, S. A. Enhanced Third Harmonic Generation in Single Germanium Nanodisks Excited at the Anapole Mode. *Nano Lett.* **2016**, *16*, 4635−4640.

(28) Shorokhov, A. S.; Melik-Gaykazyan, E. V.; Smirnova, D. A.; Hopkins, B.; Chong, K. E.; Choi, D. Y.; Shcherbakov, M. R.; Miroshnichenko, A. E.; Neshev, D. N.; Fedyanin, A. A.; Kivshar, Y. S. Multifold Enhancement of Third-Harmonic Generation

in Dielectric Nanoparticles Driven by Magnetic Fano Resonances. *Nano Lett.* **2016**, *16*, 4857−4861.

(29) Wang, L.; Kruk, S.; Xu, L.; Rahmani, M.; Smirnova, D.; Solntsev, A.; Kravchenko, I.; Neshev, D.; Kivshar, Y. Shaping the Third-Harmonic Radiation from Silicon Nanodimers. *Nanoscale* **2017**, *9*, 2201-2206.

(30) Grinblat, G.; Li, Y.; Nielsen, M. P.; Oulton, R. F.; Maier, S. A. Efficient Third Harmonic Generation and Nonlinear Sub-Wavelength Imaging at a Higher-Order Anapole Mode in a Single Germanium Nanodisk. *ACS Nano* **2017**, *11*, 953–960.

(31) Gongora, J. S. T.; Miroshnichenko, A. E.; Kivshar, Y. S.; Fratalocchi, A. Anapole Nanolasers for Mode-Locking and Ultrafast Pulse Generation. *Nat. Commun.* **2017**, *8*, 15535.

(32) Liu, S.; Ihlefeld, J. F.; Dominguez, J.; Gonzales, E. F.; Eric Bower, J; Burckel, D. B.; Sinclair, M. B.; Brener, I. Realization of Tellurium-Based All Dielectric Optical Metamaterials using a Multi-Cycle Deposition-Etch Process. *Appl. Phys. Lett.* **2013**, *102*, 161905.

(33) Zhang, L.; Agarwal, A.M.; Kimerling, L. C.; Michel, J. Nonlinear Group IV photonics based on silicon and germanium: from near-infrared to mid-infrared. *Nanophotonics* **2014**, 3, 247– 68.

(34) Boyd, R. W. In Handbook of Laser Technology and Applications; Webb, C., Jones, J., Eds.; IOP Publishing, 2004; 161−184.

(35) Zhang, L.; Agarwal, A.M.; Kimerling, L. C.; Michel, J. Nonlinear Group IV photonics based on silicon and germanium: from near-infrared to mid-infrared. *Nanophotonics* **2014**, 3, 247– 68.

(36) Hajisalem, G.; Hore, D. K.; Gordon, R. Interband Transition Enhanced Third Harmonic Generation from Nanoplasmonic Gold. Opt. *Mater. Express* **2015**, *5*, 2217−2224.

(37) Metzger, B.; Schumacher, T.; Hentschel, M.; Lippitz, M.; Giessen, H. Third Harmonic Mechanism in Complex Plasmonic Fano Structures. *ACS Photonics* **2014**, *1*, 471−476.

(38) Lippitz, M.; van Dijk, M. A.; Orrit, M. Third-Harmonic Generation from Single Gold Nanoparticles. *Nano Lett.* **2005**, *5*, 799− 802.

(39) Shibanuma, T.; Grinblat, G.; Albella, P.; Maier, S. A. Efficient Third Harmonic Generation from Metal–Dielectric Hybrid Nanoantennas. *Nano Lett.* **2017**, *17*, 2647-2651.

(40) Palik, E. D. Handbook of optical constants of solids; Academic Press: New York, 1998.

Table of contents